Nanoscale

ROYAL SOCIETY OF CHEMISTRY

COMMUNICATION

View Article Online
View Journal | View Issue

Cite this: *Nanoscale*, 2021, **13**, 13610

Received 31st May 2021,
Accepted 17th July 2021

DOI: 10.1039/d1nr03471e

rsc.li/nanoscale

Highly efficient photothermal nanoparticles for the rapid eradication of bacterial biofilms†

Wei He,‡[a,c] Zaiyu Wang,‡[a] Haotian Bai,[a] Zheng Zhao,[b] Ryan T. K. Kwok,*[a,c] Jacky W. Y. Lam[a,c] and Ben Zhong Tang*[a,b,c,d]

Biofilm-related infections, such as dental plaque, chronic sinusitis, native valve endocarditis, and chronic airway infections in cystic fibrosis have brought serious suffering to patients and financial burden to society. Materials that can eliminate mature biofilms without developing drug resistance are promising tools to treat biofilm-related infections, and thus they are in urgent demand. Herein, we designed and readily prepared organic nanoparticles (NPs) with highly efficient photothermal conversion by harvesting energy *via* excited-state intramolecular motions and enlarging molar absorptivity. The photothermal NPs can sufficiently eliminate mature bacterial biofilms upon low-power near-infrared laser irradiation. NPs hold great promise for the rapid eradication of bacterial biofilms by photothermal therapy.

Introduction

Biofilm-related infections, such as dental plaque, chronic otitis media, chronic sinusitis, native valve endocarditis, and chronic airway infections in cystic fibrosis have brought serious suffering to patients and heavy financial burden to society.[1–3] Moreover, microbial adhesion and biofilm formation on implants and devices account for more than 50% of all nosocomial infections, including urinary tract, percutaneous, subcutaneous, soft tissue, eyes, circulatory system, and bones.[4–6] Bacterial biofilm is a unified community where bacterial cells are encapsulated by the matrix, extracellular polymeric substance (EPS), which is composed of protein, polysaccharides, and extracellular DNAs.[7] Bacteria within a mature biofilm usually show stronger resistance to antibiotics compared to their planktonic relatives.[8,9] On the one hand, EPS confers a physical barrier to protect biofilm from antibiotics and disinfectants in the outer environment. On the other hand, quorum sensing of biofilm cells is a powerful method to build drug resistance by efficient communication to each other in the EPS-embedded biofilms.[10,11] It has been reported that up to 1000-fold antibiotics dosage is required to treat biofilms compared to the individual bacteria,[12,13] resulting in severe multi-drug resistance (MDR) generation in practice. Therefore, new and much powerful antibiotics are required to treat the MDR-biofilms. However, the research and development of new effective antibiotics are time-consuming; therefore, new strategies for combating biofilms are highly desired.

To deal with this challenge, several materials for biofilm disruption and detachment have been developed, such as cationic molecules, water-soluble conjugated polymers, proteases, DNase, D-amino acids, anti-biofouling nanopatterned surfaces, and photoactive materials.[13–21] Cationic molecules were usually applied for the destruction of bacteria in the biofilm through electrostatic interactions.[14] Repeated light absorbing units in conjugated polymers allow the excitation energy transfer along the whole backbone to the acceptor, resulting in the amplified utilization rate of light energy, which significantly improves the killing efficiency toward bacteria embedded in the matrix.[16] Enzymes such as proteases and DNase can degrade the proteins and extracellular DNA in biofilm matrix.[19] However, they are not specific enough to differentiate bacterial infection sites from normal living tissues. Bioactive D-amino acids are promising treatment reagents for anti-biofouling surfaces. It has been reported that D-leucine,

[a]*Department of Chemistry, Hong Kong Branch of Chinese National Engineering Research Center for Tissue Restoration and Reconstruction, The Hong Kong University of Science and Technology, Clear Water Bay, KowloonHong Kong, China. E-mail: chryan@ust.hk, tangbenz@ust.hk*
[b]*Shenzhen Institute of Molecular Aggregate Science and Engineering, School of Science and Engineering, The Chinese University of Hong Kong, Shenzhen, 2001 Longxiang Boulevard, Longgang District, Shenzhen City, Guangdong 518172, China*
[c]*HKUST Shenzhen Research Institute, No. 9 Yuexing 1st RD, South Area Hi-tech Park, Nanshan, Shenzhen 518057, China*
[d]*State Key Laboratory of Luminescent Materials and Devices, and Center for Aggregation-Induced Emission (Guangzhou International Campus), South China University of Technology, Guangzhou 510640, China*
†Electronic supplementary information (ESI) available. See DOI: 10.1039/d1nr03471e
‡These authors contributed equally.

D-methionine, D-tyrosine, and D-tryptophan produced by *Bacillus subtilis* were found to prevent biofilm formation and break down existing biofilms by releasing the amyloid fibers that linked cells in the biofilm together.[18] Nevertheless, spatiotemporal control of D-amino acids remains a difficult task for further applications. Anti-fouling nanopatterned surfaces work as another solution track for efficiently controlling bio-interfacial interactions with bacteria.[21] Thermo-responsive polymer brushes and biocidal polymer brushes, usually containing quaternary ammonium salt as working moiety, were applied as spacing/releasing regions and contacting/killing regions, respectively. By tuning the temperature, killing and releasing bacteria could be realized in a controllable way.[21] Despite the outstanding controllable characteristics, the construction of the nanopatterned surfaces is rather difficult and is limited to a small scale. Therefore, light controllable theranostics systems, *i.e.*, photodynamic therapy (PDT) and photothermal therapy (PTT) have attracted considerable research attentions.[22–26] PDT is mainly based on the materials that can efficiently generate reactive oxygen species (ROS) upon light excitation.[27] Many investigations have been carried out to destroy biofilms. Unfortunately, ROS could cause some side effects, such as acute inflammation. Meanwhile, laser-induced hyperthermia based on near-infrared (NIR) light-absorbing nanoagents has become one of the most attractive strategies for combating bacteria. The killing of microbes based on photothermal materials that are capable of converting light into heat to destroy bacteria by denaturation of their cell wall, proteins, and enzymes,[28] shows advantages over traditional antibacterial approaches.[29,30]

In recent years, the potential application of PTT based on NIR irradiation has gained increasing attention in the field of nanomedicine due to its minimal invasiveness, deep tissue penetration, and high spatiotemporal selectivity.[31] Moreover, PTT has been recognized as a promising antibacterial strategy through local hyperthermia to destroy bacterial cell integrity or biofilm structure.[32,33] As for the antibacterial application of PTT, graphene, gold nanoparticles, CuS nanodots, and MoS_2 nanosheets were successfully developed.[20,24] Remarkably, organic π-conjugated molecules or polymers are emerging as competitive photothermal agents, owing to their excellent biocompatibility, easily tunable bandgap, and accessible structural-property relationships. Some popularly used molecules, such as indocyanine green (ICG) and methylene blue (MB), have been approved by the FDA for clinical use.[34,35] However, these kinds of planar molecules have very strong face-to-face π–π stacking interactions in the aggregate state, resulting in both insufficient radiative decay and nonradiative decay.[36] Our group recently proposed some new molecular design strategies to manipulate molecular motions in the solution/aggregate state and enhance the molar absorptivity.[37,38] 2TPE-2NDTA nanoparticles with highly boosted photothermy by virtue of internally efficient excited-state intramolecular motions were successfully developed.[37] In addition, a NIR-emissive molecule, TDADT with high molar absorptivity, acceptable quantum yield, and sizeable photothermal conversion efficiency was developed for *in vivo* NIR-II imaging-guided cancer surgery and NIR-I photothermal therapy.[38] These photothermal systems also hold a great promise in treating bacterial biofilms in NIR window remotely.

Herein, we report a highly efficient photothermal nanoparticle to combat biofilms with molecular aggregates that exhibit excellent photothermal generation by taking advantage of active intramolecular motions in the aggregate state and enhanced molar absorptivity. A NIR-absorbing organic nanoparticle, namely TN NPs with slight structural modification of reported 2TPE-2NDTA NPs, has been rationally designed and fabricated based on previous reports (Scheme 1).[37,38] TN NPs showed high ability in photothermal conversion and good photobleaching resistance. The prepared NPs can effectively eliminate mature *S. aureus* biofilms upon NIR laser (808 nm, 1 W cm^{-1}) irradiation while exerting no toxicity to the biofilms in the dark, suggesting this photothermal nanoparticle system holds great potential in compacting biofilm-related infections *via* photothermy. The elimination mechanism of TN NPs was proposed to be a synergetic deactivated path, in which aggregates located in the matrix instead of targeting an individual cell, and the heat generated by the NPs destroyed the adjacent bacteria cells. At the same time, the photothermy also deactivated the adhesive components, such as proteins, polysaccharides, and extracellular DNAs in the matrix, leading to the disassembly of mature biofilms.

Results and discussion

Photophysical properties of 2TPE-2NDTA-02 (TN) and its DSPE-PEG-encapsulated NPs

2TPE-2NDTA-02 (TN) was synthesized according to the previous work (Scheme S1†).[37] To fabricate NIR-activated photothermal NPs, TN was doped into 1,2-distearoyl-*sn-glycero*-3-phosphoethanolamine-*N*-[methoxy(poly(ethylene glycol))-2000] ($DSPE\text{-}PEG_{2000}$) by the nano-precipitation method, as illustrated in Fig. 1A. Light absorption is requisite for eligible photothermal materials. As shown in Fig. 1B and C, TN NPs possessed a NIR-absorption region up to 950 nm and the emission peak is located at around 1071 nm under 800 nm NIR laser excitation. According to the intramolecular motion-induced photothermy (iMIPT) mechanism[37] and enlarging absorption reservoir strategy,[38] the TN molecules showed high molar absorptivity (ε) (Fig. S1†) while its fluorescence was weak in the aggregate state (Fig. 1C), indicating the high photothermal conversion potential. In the aggregate state, the absorption peak was red shifted from 660 nm to 728 nm compared with its profile in solution, owing to the presence of intermolecular interactions within aggregates (Fig. S2†). Moreover, the physical properties of TN NPs were further evaluated. The particle size was 120 ± 2.1 nm, as determined by dynamic light scattering (DLS) and TEM analysis (Fig. 1D). The zeta potential of NPs was found to be −57 ± 0.2 mV that was suitable for biofilm matrix targeting. A negative sheath layer could help NPs become invisible and penetrate to a deeper

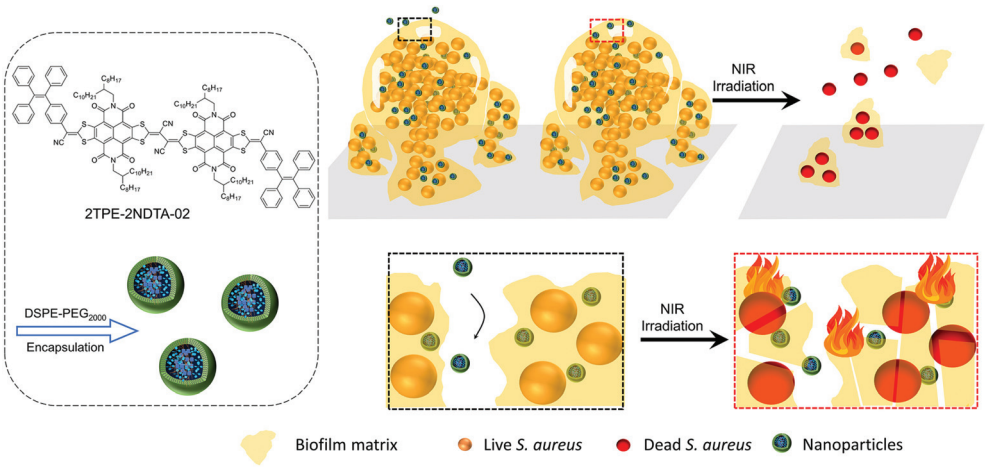

Scheme 1 DSPE-PEG encapsulated 2TPE-2NDTA-02 (TN) NPs for eradication of mature bacterial biofilms by photothermal effect.

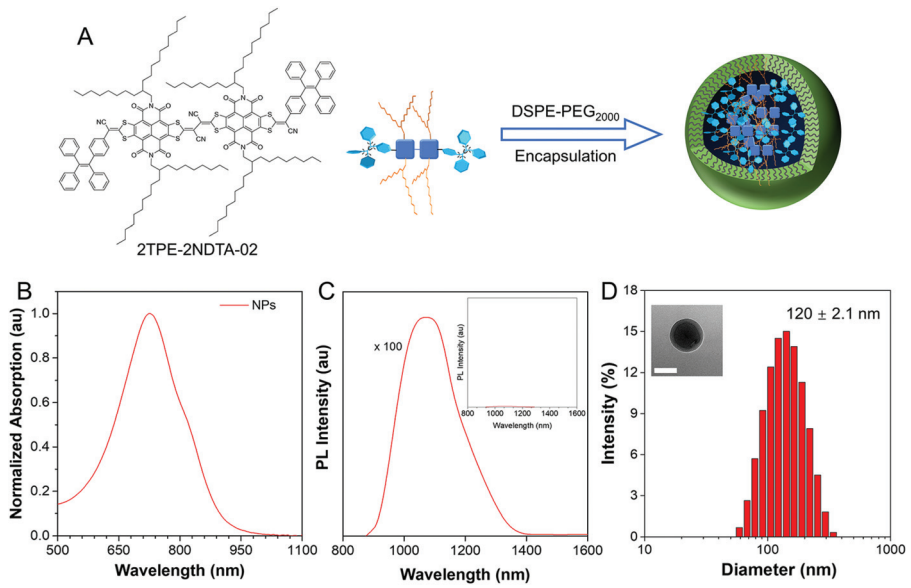

Fig. 1 (A) Schematic illustrations of fabrication of TN NPs by encapsulating DSPE-PEG$_{2000}$ with 2TPE-2NDTA-02. (B) Normalized absorption spectrum of TN NPs. (C) PL spectra of TN NPs. Concentration: 100 μM (based on TN); λ_{ex} = 820 nm. (D) DLS histogram and TEM image of TN NPs. Scale bar: 100 nm.

position in biofilms with fewer interactions with bacterial cells.[13,39] Besides, the size of the NPs did not change for 6 months (Fig. S3†), indicating the good colloidal stability of NPs over time.

Photothermal conversion efficiency of TN NPs

The photothermal conversion ability of TN NPs was investigated. As shown in Fig. 2A, 100 μM NPs can easily reach up to above 70 °C after NIR laser irradiation (808 nm, 1 W cm^{-2}) for 5 min. While the temperature of the water control merely changed even after 5 min irradiation, indicating that the photothermal effect was solely caused by the TN molecules in the nanoparticles. To determine photothermal conversion capability of TN NPs, aqueous suspensions with TN NPs of different concentrations were irradiated utilizing NIR laser with 808 nm at 1 W cm^{-2}, and temperature information was recorded by the IR thermal camera. The temperatures of the aqueous solutions of all NPs elevated with time and reached a maximum within 3 min (Fig. 2B). The plateau photothermal temperatures of different concentrations of TN NPs were 70.5 °C (100 μM), 59.1 °C (50 μM), 42.6 °C (25 μM), 36.9 °C (12.5 μM), and 30.6 °C (6.25 μM) respectively. In addition, TN NPs represented a good relation between concentration and photothermal conversion within the range from 0 to 100 μM, giving a great potential for designing and speculating temperature in specific biological applications.

Previous research has proved that bacteria can be effectively killed at high temperatures, where 60–70 °C could be regarded

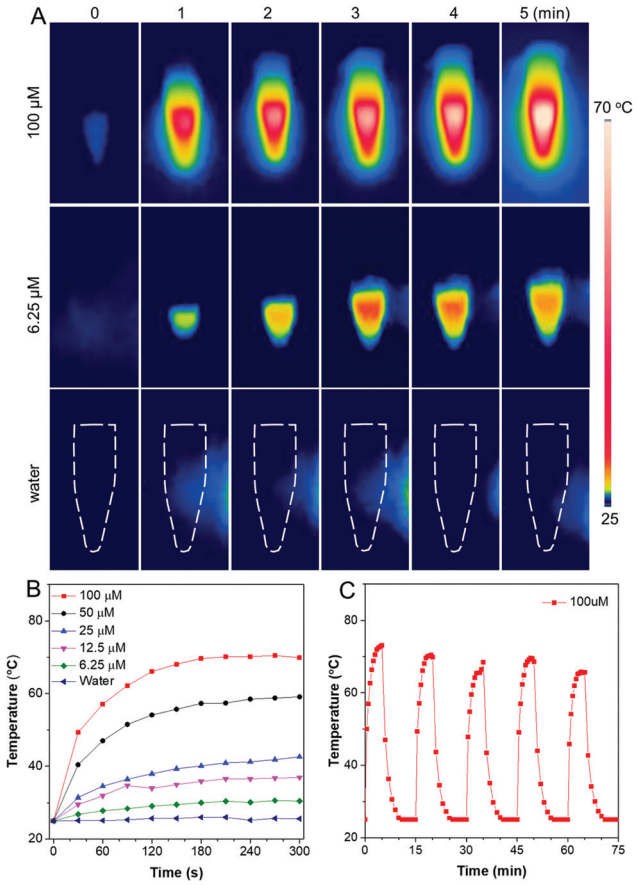

Fig. 2 Photothermal properties of TN NPs. (A) IR thermal images of various TN NPs in aqueous solution (100 μM based on TN) and water upon exposure to 808 nm (1 W cm^{-2}) laser irradiation at different time intervals. (B) Photothermal conversion behavior of TN NPs in aqueous solution at different concentrations (0, 6.25, 12.5, 25, 50, and 100 μM) under 808 nm laser (1 W cm^{-2}) irradiation. (C) Temperature changes in solutions of TN NPs as a function of time. The solutions were irradiated with 808 nm laser (1 W cm^{-2}) for 5 min followed by naturally cooling for another 10 min.

as the most suitable temperature window for efficient removal of adherent bacteria or biofilms.[40] Therefore, 100 μM of TN NPs should be the optimum concentration for the antibiofilm study. According to the calculation methods of photothermal conversion efficiency reported in the literature,[37,41] the photothermal conversion efficiency (PCE) of TN NPs was calculated to be around 28.0%. Such excellent photothermal conversion behavior is attributed to the strong light absorptivity and effective excited-state intramolecular motion within NPs that considerably convert the absorbed light energy for heat production. Furthermore, the photothermal properties of TN NPs were almost invariable after five laser-irradiation cycles (continuous irradiation for 5 min followed by naturally cooling for another 10 min), indicating a strong resistance to photobleaching (Fig. 2C). Photothermy conversion characteristics were also stable in 96-well plates, where bacterial biofilm model would be inoculated into (Fig. S4†). The TN NPs could work as an organic photothermal reagent with stable hydrodynamic size, high molar absorptivity, and high PCE (28.0% at 808 nm). All these superior properties make TN NPs promising for the eradication of bacterial biofilms with comprehensive architectures and a thick sticky matrix.

Antibiofilm ability of TN NPs

In addition, we evaluated the effect of TN NPs based antibacterial system on the dispersion of stubborn film using *S. aureus* as a model, which is prone to form biofilms on the surface of biomaterial implants.[42] 100 μM of TN NPs were adopted to treat mature *S. aureus* biofilms. The method of crystal violet (CV) staining was employed to quantify the biomass.[43,44] CV is a basic dye and binds to negatively charged surface molecules and polysaccharides in the extracellular matrix.[45] As per the results shown in Fig. 3A and B, TN NPs together with NIR irradiation could remarkably reduce the biomass of biofilm by about 75%, whereas TN NPs or NIR laser alone did not display distinct effects towards the biofilm. *In situ* IR images (Fig. 3C) in a 96-well plate further indicated that the combination of TN NPs and NIR irradiation played a prominent role in the photothermal effect. The high destructive and inhibition effects result from the photoconversion to heat that destroyed the biofilm components, including

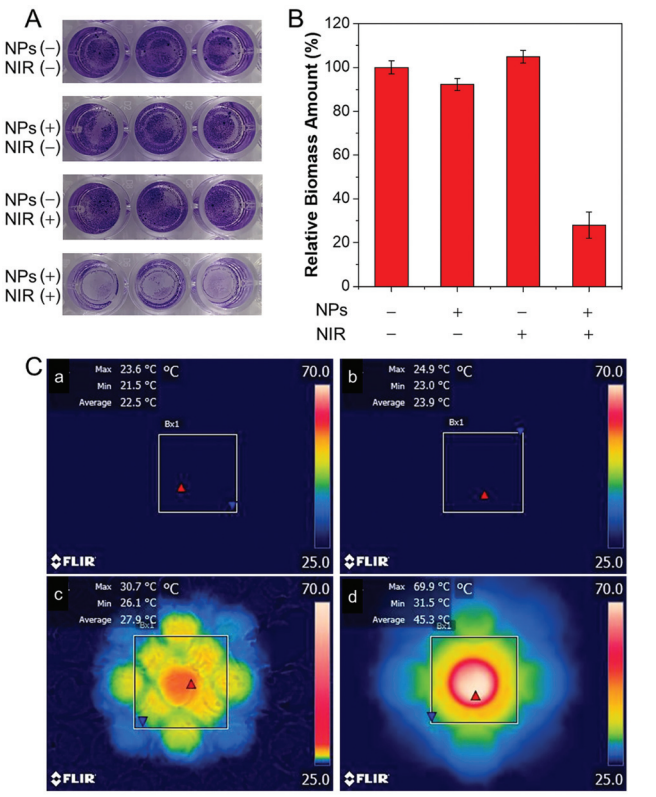

Fig. 3 (A) Digital images of *S. aureus* biofilms stained with 0.1% (w/w) crystal violet (CV) after treatment under different conditions. (B) Relative biomass amount of each group. (C) IR images of (a) blank *S. aureus* biofilm without any treatment; (b) the biofilm only treated with TN NPs; (c) the biofilm only treated with NIR irradiation for 10 min; (d) the biofilm treated with TN NPs and NIR irradiation for 10 min. The concentration of TN NPs was 100 μM and the NIR irradiation time was 10 min.

embedded bacterial cells and matrix, which is mainly composed of proteins, polysaccharides, and extracellular nucleic acids. The CV assay further supported that this photothermal nanoparticle system showed high potential for the eradication of mature biofilms.

Since all bacterial cells, including both live and dead, as well as matrix, were counted by CV, the assay cannot directly reflect the killing effects of biofilm cells.[33] Therefore, plate count experiments were carried out to investigate the killing effect on biofilm cells (Fig. 4A). Biofilms were treated under the same conditions as the previous experiment except for the final washing step. After NIR irradiation, all the biofilms were re-suspended in 1 × PBS buffer. It was found that the number of colony-forming units (CFU) per well values reduced over 7-log-unit when TN NPs and NIR irradiation were employed. Simultaneously, the biofilm dispersion effect was easily observed by confocal laser scanning microscope (CLSM). The biofilm was stained with BacLight Live/Dead Kit, where live *S. aureus* was stained with green fluorescence, and dead bacteria were stained with red fluorescence. As shown in Fig. 4C–E, the mature biofilm in the control groups was held together and possessed three-dimensional structures with a thickness of around 20 μm. In contrast, there was a small number of residual bacteria after treatment with TN NPs and NIR irradiation (Fig. 4F), indicating that NPs showed excellent dispersion ability to *S. aureus*. On the other hand, all the residual bacteria on the cover glass were identified to be dead ones in the propidium iodine (PI) channel, as demonstrated in Fig. 4G, indicating the heat generated by the TN NPs system could also kill the bacteria efficiently.

Finally, we studied the photothermal effect towards the extracellular polymeric substance (EPS) matrix in the mature biofilm model. SEM and biofilm matrix probes were employed for investigation. FilmTracer SYPRO Ruby (FTSR) preferentially binds to proteins, which are the components offering structural stability to biofilms.[46,47] Therefore, signal intensities of the FTSR probe provide insights into the EPS matrix. Fig. 5A–D showed the SEM images of the biofilms treated under different conditions. The morphologies of biofilms in Fig. 5A–C showed

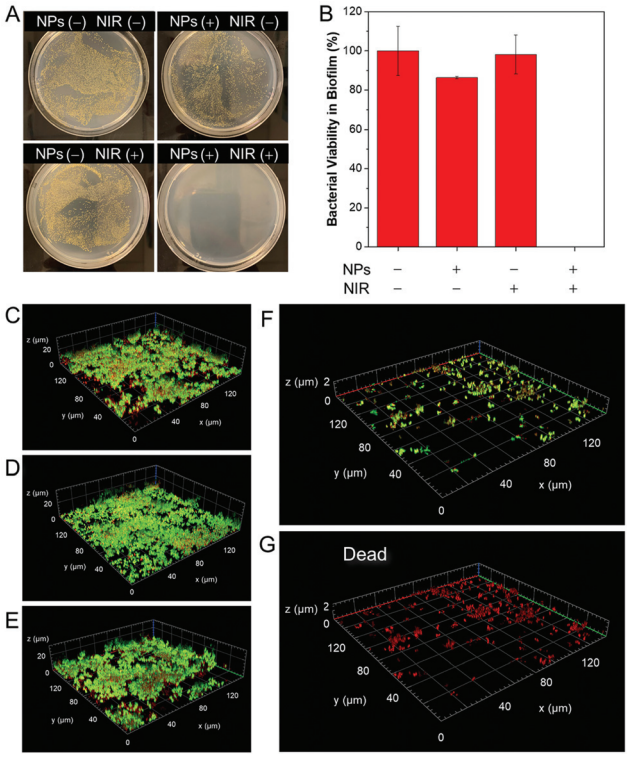

Fig. 4 Photothermal-induced bacterial cell death in mature *S. aureus* biofilms. (A) Digital images of live *S. aureus* colonies grown on NB agar. (B) Relative bacterial cell viability in the treated biofilm of each group. (C–G) Bacterial viability measurement of the treated biofilms, where (C) the biofilm was neither treated with TN NPs nor NIR irradiation, (D) the biofilm was only treated with TN NPs, (E) the biofilm was only treated with NIR irradiation, and (F and G) the biofilm was treated with both TN NPs and NIR irradiation. Green fluorescence and red fluorescence represented live and dead *S. aureus*, respectively. The concentration of TN NPs was 100 μM and the NIR irradiation time was 10 min.

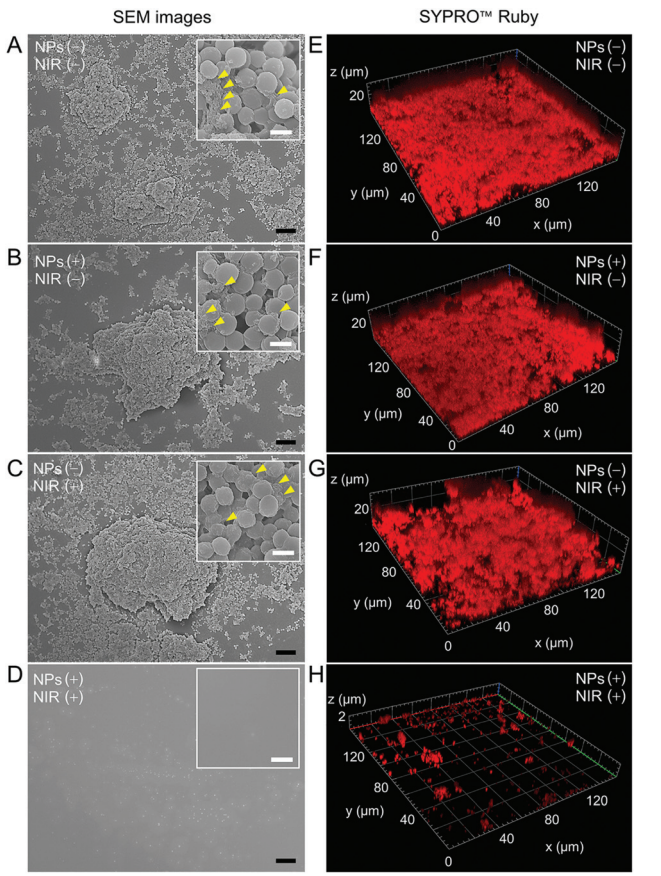

Fig. 5 Photothermal-induced dissociation of the matrix in mature biofilms. Left panel: SEM images of various biofilms, where yellow arrows indicated the EPS matrix in mature biofilms. Black scale bar: 10 μm. White scale bar: 1 μm. Right panel: biofilms stained with FilmTracer SYPRO Ruby Biofilm Matrix Stain. (A and E) biofilm without treatment; (B and F) biofilm was only treated with TN NPs; (C and G) biofilm was only treated with NIR irradiation; (D and H) biofilm treated with TN NPs and NIR irradiation. The concentration of TN NPs was 100 μM and the NIR irradiation time was 10 min.

the typical three-dimensional (3D) characteristics of biofilms in which the *S. aureus* organized themselves into a sticky and multicellular community. EPS matrix was observed in these three groups (indicated by yellow arrows), whereas no trace of the biofilm was found in the group treated with both TN NPs and NIR irradiation (Fig. 5D), demonstrating that the mature biofilm was significantly removed. The results from FTSR staining were in agreement with those obtained from SEM microscopy. In Fig. 5E–G, the abundant fluorescence signal from FTSR and obvious morphologies were recorded in 3D CLSM images, suggesting a large amount of EPS matrix in the first three groups. It could be found that the height of biofilms could exceed 20 μm. While only sporadic dot-like signals could be found on the surface (Fig. 5H), indicating the components providing structural stability to biofilms in the EPS matrix had been either destroyed or removed.

Conclusions

An effective photothermy generation organic system in an aggregate-state for biofilm elimination was successfully developed. The TN NPs exhibited high photothermal conversion efficiency and excellent photobleaching resistance. Upon 5 min NIR irradiation, the aqueous solution of TN NPs reached a maximum of 70 °C, and the maximum temperature was unchanged after 5 measurement cycles. The TN NPs themselves exerted no toxicity towards the biofilms but effectively eliminated the mature *S. aureus* biofilms upon NIR irradiation for 10 min. This photothermal nanoaggregate system could destroy the biofilm matrix and kill the embedded cells at the same time, indicating it could be a promising photothermal agent for treating various biofilm infections.

Author contributions

W.H. and Z. W. contributed equally. W. H. conceived the original idea for this study. W. H. designed the experiments. W. H., Z. W. and Z. Z. designed the molecules. Z. W. and Z. Z synthesized the molecules. W. H. did all the experiments, including photophysical measurements, nanoparticle preparation, bacterial culture, photothermal eradication of biofilms, characterization, and calculation. H. B. helped to do dynamic laser scattering experiments and revise the manuscript. B. Z. T. supervised the whole process. R. T. K. K. co-supervised the project. B. Z. T., W. H., Z. W., Z. Z., H. B. and R. T. K. K. discussed and prepared the manuscript. W. H. wrote the manuscript, and H. B. and R. T. K. K. revised the manuscript. All authors participated in data analysis. All authors have approved the final version of the manuscript.

Conflicts of interest

There are no conflicts to declare.

Acknowledgements

This work is supported by the National Science Foundation of China (21788102), Research Grants Council of Hong Kong (N_HKUST609/19 and C6009-17G), the Innovation and Technology Commission (ITC-CNERC14SC01), and the National Key Research and Development program of China (2018YFE0190200), the Science and Technology Plan of Shenzhen (JCYJ20200109110608167, JCYJ20180507183832744, and JCYJ20180306180231853).

Notes and references

1 H. J. Busscher, H. C. van der Mei, G. Subbiahdoss, P. C. Jutte, J. J. van den Dungen, S. A. Zaat, M. J. Schultz and D. W. Grainger, *Sci. Transl. Med.*, 2012, **4**, 153rv10.
2 L. Yuwen, Y. Sun, G. Tan, W. Xiu, Y. Zhang, L. Weng, Z. Teng and L. Wang, *Nanoscale*, 2018, **10**, 16711–16720.
3 M. Chen, J. Wei, S. Xie, X. Tao, Z. Zhang, P. Ran and X. Li, *Nanoscale*, 2019, **11**, 1410–1422.
4 R. A. Weinstein and R. O. Darouiche, *Clin. Infect. Dis.*, 2001, **33**, 1567–1572.
5 S. Young, S. A. Lie, G. Hallan, L. G. Zirkle, L. B. Engesaeter and L. I. Havelin, *Acta Orthop.*, 2011, **82**, 737–743.
6 K. G. Neoh, X. Hu, D. Zheng and E. T. Kang, *Biomaterials*, 2012, **33**, 2813–2822.
7 H. C. Flemming, J. Wingender, U. Szewzyk, P. Steinberg, S. A. Rice and S. Kjelleberg, *Nat. Rev. Microbiol.*, 2016, **14**, 563–575.
8 D. Lebeaux, J. M. Ghigo and C. Beloin, *Microbiol. Mol. Biol. Rev.*, 2014, **78**, 510–543.
9 T. Bottcher, I. Kolodkin-Gal, R. Kolter, R. Losick and J. Clardy, *J. Am. Chem. Soc.*, 2013, **135**, 2927–2930.
10 A. Smith, *Adv. Drug Delivery Rev.*, 2005, **57**, 1539–1550.
11 J. A. Thompson, R. A. Oliveira, A. Djukovic, C. Ubeda and K. B. Xavier, *Cell Rep.*, 2015, **10**, 1861–1871.
12 T.-F.C. Mah and G. A. O'Toole, *Trends Microbiol.*, 2001, **9**, 34–39.
13 Y. Zhao, X. Dai, X. Wei, Y. Yu, X. Chen, X. Zhang and C. Li, *ACS Appl. Mater. Interfaces*, 2018, **10**, 14426–14437.
14 Q. Wang, L. Wang, L. Gao, L. Yu, W. Feng, N. Liu, M. Xu, X. Li, P. Li and W. Huang, *J. Mater. Chem. B*, 2019, **7**, 3865–3875.
15 T. E. Angelini, M. Roper, R. Kolter, D. A. Weitz and M. P. Brenner, *Proc. Natl. Acad. Sci. U. S. A.*, 2009, **106**, 18109–18113.
16 P. Zhang, S. Li, H. Chen, X. Wang, L. Liu, F. Lv and S. Wang, *ACS Appl. Mater. Interfaces*, 2017, **9**, 16933–16938.
17 C. B. Whitchurch, T. Tolker-Nielsen, P. C. Ragas and J. S. Mattick, *Science*, 2002, **295**, 1487–1487.
18 I. Kolodkin-Gal, D. Romero, S. Cao, J. Clardy, R. Kolter and R. Losick, *Science*, 2010, **328**, 627–629.
19 T. K. Lu and J. J. Collins, *Proc. Natl. Acad. Sci. U. S. A.*, 2007, **104**, 11197–11202.

20 W. Yin, J. Yu, F. Lv, L. Yan, L. R. Zheng, Z. Gu and Y. Zhao, *ACS Nano*, 2016, **10**, 11000–11011.
21 Q. Yu, J. Cho, P. Shivapooja, L. K. Ista and G. P. Lopez, *ACS Appl. Mater. Interfaces*, 2013, **5**, 9295–9304.
22 X. Jia, I. Ahmad, R. Yang and C. Wang, *J. Mater. Chem. B*, 2017, **5**, 2459–2467.
23 P. Pallavicini, A. Dona, A. Taglietti, P. Minzioni, M. Patrini, G. Dacarro, G. Chirico, L. Sironi, N. Bloise, L. Visai and L. Scarabelli, *Chem. Commun.*, 2014, **50**, 1969–1971.
24 Z. Yuan, B. Tao, Y. He, C. Mu, G. Liu, J. Zhang, Q. Liao, P. Liu and K. Cai, *Biomaterials*, 2019, **223**, 119479.
25 D. Hu, H. Li, B. Wang, Z. Ye, W. Lei, F. Jia, Q. Jin, K. F. Ren and J. Ji, *ACS Nano*, 2017, **11**, 9330–9339.
26 M. Kang, Z. Zhang, N. Song, M. Li, P. Sun, X. Chen, D. Wang and B. Z. Tang, *Aggregate*, 2020, **1**, 80–106.
27 Z. Zhou, J. Song, L. Nie and X. Chen, *Chem. Soc. Rev.*, 2016, **45**, 6597–6626.
28 P. C. Ray, S. A. Khan, A. K. Singh, D. Senapati and Z. Fan, *Chem. Soc. Rev.*, 2012, **41**, 3193–3209.
29 L. Hui, J. T. Auletta, Z. Huang, X. Chen, F. Xia, S. Yang, H. Liu and L. Yang, *ACS Appl. Mater. Interfaces*, 2015, **7**, 10511–10517.
30 R. Tejero, D. Lopez, F. Lopez-Fabal, J. L. Gomez-Garces and M. Fernandez-Garcia, *Biomacromolecules*, 2015, **16**, 1844–1854.
31 L. Cheng, C. Wang, L. Feng, K. Yang and Z. Liu, *Chem. Rev.*, 2014, **114**, 10869–10939.
32 M.-C. Wu, A. R. Deokar, J.-H. Liao, P.-Y. Shih and Y.-C. Ling, *ACS Nano*, 2013, **7**, 1281–1290.
33 X. Cai, D. Mao, C. Wang, D. Kong, X. Cheng and B. Liu, *Angew. Chem., Int. Ed.*, 2018, **57**, 16396–16400.
34 W. W. Gärtner, *Phys. Rev.*, 1961, **122**, 419–424.
35 J. T. Alander, I. Kaartinen, A. Laakso, T. Patila, T. Spillmann, V. V. Tuchin, M. Venermo and P. Valisuo, *Int. J. Biomed. Imaging*, 2012, **2012**, 940585.
36 S. M. Fateminia, Z. Wang, C. C. Goh, P. N. Manghnani, W. Wu, D. Mao, L. G. Ng, Z. Zhao, B. Z. Tang and B. Liu, *Adv. Mater.*, 2017, **29**, 1604100.
37 Z. Zhao, C. Chen, W. Wu, F. Wang, L. Du, X. Zhang, Y. Xiong, X. He, Y. Cai, R. T. K. Kwok, J. W. Y. Lam, X. Gao, P. Sun, D. L. Phillips, D. Ding and B. Z. Tang, *Nat. Commun.*, 2019, **10**, 768.
38 Y. Li, J. Zhang, S. Liu, C. Zhang, C. Chuah, Y. Tang, R. T. K. Kwok, J. W. Y. Lam, H. Ou, D. Ding and B. Z. Tang, *Adv. Funct. Mater.*, 2021, 2102213.
39 A. S. Messiaen, K. Forier, H. Nelis, K. Braeckmans and T. Coenye, *PLoS One*, 2013, **8**, e79220.
40 W. Lei, K. Ren, T. Chen, X. Chen, B. Li, H. Chang and J. Ji, *Adv. Mater. Interfaces*, 2016, **3**, 1600767.
41 S. Li, Q. Deng, Y. Zhang, X. Li, G. Wen, X. Cui, Y. Wan, Y. Huang, J. Chen, Z. Liu, L. Wang and C. S. Lee, *Adv. Mater.*, 2020, **32**, e2001146.
42 G. Subbiahdoss, S. Sharifi, D. W. Grijpma, S. Laurent, H. C. van der Mei, M. Mahmoudi and H. J. Busscher, *Acta Biomater.*, 2012, **8**, 2047–2055.
43 G. A. O'Toole, *J. Visualized Exp.*, 2011, **47**, e2437.
44 E. Peeters, H. J. Nelis and T. Coenye, *J. Microbiol. Methods*, 2008, **72**, 157–165.
45 X. Li, Z. Yan and J. Xu, *Microbiology*, 2003, **149**, 353–362.
46 B. Jalvo, M. Faraldos, A. Bahamonde and R. Rosal, *J. Hazard. Mater.*, 2017, **340**, 160–170.
47 L. Valencia, S. Kumar, B. Jalvo, A. Mautner, G. Salazar-Alvarez and A. P. Mathew, *J. Mater. Chem. A*, 2018, **6**, 16361–16370.